

Characterisation of Weibel–Palade body fusion by amperometry in endothelial cells reveals fusion pore dynamics and the effect of cholesterol on exocytosis

Emma A. Cookson¹, Ianina L. Conte^{1,*}, John Dempster², Matthew J. Hannah³ and Tom Carter^{1,*‡}

¹MRC National Institute for Medical Research, Mill Hill, London, NW7 1AA, UK

²University of Strathclyde, Glasgow G1 1XQ, UK

³Microbiology Services Division Colindale, Public Health England, 61 Colindale Avenue, London, NW9 5EQ, UK

*Present address: Division of Biomedical Sciences, St George's, University of London, London SW17 0RE, UK

‡Author for correspondence (tcarter@nimr.mrc.ac.uk; tcarter@sgul.ac.uk)

Accepted 24 September 2013

Journal of Cell Science 126, 5490–5499

© 2013. Published by The Company of Biologists Ltd

doi: 10.1242/jcs.138438

Summary

Regulated secretion from endothelial cells is mediated by Weibel–Palade body (WPB) exocytosis. Plasma membrane cholesterol is implicated in regulating secretory granule exocytosis and fusion pore dynamics; however, its role in modulating WPB exocytosis is not clear. To address this we combined high-resolution electrochemical analysis of WPB fusion pore dynamics, by amperometry, with high-speed optical imaging of WPB exocytosis following cholesterol depletion or supplementation in human umbilical vein endothelial cells. We identified serotonin (5-HT) immunoreactivity in WPBs, and VMAT1 expression allowing detection of secreted 5-HT as discrete current spikes during exocytosis. A high proportion of spikes (~75%) had pre-spike foot signals, indicating that WPB fusion proceeds via an initial narrow pore. Cholesterol depletion significantly reduced pre-spike foot signal duration and increased the rate of fusion pore expansion, whereas cholesterol supplementation had broadly the reverse effect. Cholesterol depletion slowed the onset of hormone-evoked WPB exocytosis, whereas its supplementation increased the rate of WPB exocytosis and hormone-evoked proregion secretion. Our results provide the first analysis of WPB fusion pore dynamics and highlight an important role for cholesterol in the regulation of WPB exocytosis.

Key words: Weibel–Palade bodies, Endothelial cell, VMAT1, Serotonin, Amperometry, Exocytosis

Introduction

Weibel–Palade bodies (WPBs) are regulated secretory granules of endothelial cells (Knipe et al., 2010; Rondaj et al., 2006). WPB formation is driven by condensation of polymers of the haemostatic glycoprotein Von Willebrand factor (VWF) in association with the cleaved VWF propolypeptide (proregion) (Sadler, 1998; Springer, 2011; Wagner, 1990). Secreted VWF plays important roles in haemostasis, might modulate blood vessel growth and the spread of metastatic cancer cells, and contributes to thrombosis under pathological conditions (Sadler, 1998; Starke et al., 2011; Terraube et al., 2007). WPB exocytosis is also a main route for regulated secretion of proteins modulating inflammation, blood vessel tone and vessel growth and remodelling (Rondaj et al., 2006; van Breevoort et al., 2012).

Physical, mechanical and/or chemical signals generated during vessel injury, stress or infection trigger WPB exocytosis, primarily through elevating intracellular free calcium ion ($[Ca^{2+}]_i$) and/or cAMP concentrations (Rondaj et al., 2006). Key molecules involved in the delivery, docking and exocytosis of WPBs have been identified (Bierings et al., 2012; Fu et al., 2005; König et al., 1998; Nightingale et al., 2009; Pulido et al., 2011; Rojo Pulido et al., 2011; Zografou et al., 2012); however,

little is known about the processes regulating the final stages of WPB exocytosis, in particular the dynamics of the fusion pore connecting the WPB lumen with the extracellular space. Fusion pore dynamics are modulated by Ca^{2+} , proteins and membrane lipids, such as cholesterol (Anantharam et al., 2011; Berberian et al., 2009; Chang et al., 2009; Fang et al., 2008; Ge et al., 2010; Jackson and Chapman, 2008; Neco et al., 2008; Segovia et al., 2010; Wang et al., 2010; Zimmerberg and Chernomordik, 2005). Regulation of fusion pore dynamics is thought to influence both the extent and composition of secreted cargo (Braun et al., 2007; Obermüller et al., 2005; Soekmadji and Thorn, 2010); Vardjan et al., 2009; Vardjan et al., 2007), a process recently reported to occur during WPB exocytosis (Babich et al., 2008). Although high levels of circulating cholesterol are associated with elevated plasma VWF (Blann et al., 1995; Pérez-Jiménez et al., 1999), a risk factor for thrombosis and stroke (Jansson et al., 1991; Qizilbash et al., 1997), it remains unclear whether endothelial cell plasma membrane cholesterol modulates WPB fusion pore dynamics or stimulated cargo secretion.

Fusion pores form on a millisecond time scale and require specialised approaches for their detection. Where secretory granules contain diffusible oxidisable molecules, e.g. monoamines, fusion pore formation and expansion can be resolved as current spikes using carbon fibre amperometry (amperometry) (Chow and Von Ruden, 2009). The shape of an

amperometric current spike can provide direct mechanistic information about the underlying process of membrane fusion, including the initial formation of the fusion pore, seen as a small increase in current preceding the main spike and termed the pre-spike foot signal (Alvarez de Toledo et al., 1993; Chow et al., 1992).

Here, we report that human umbilical vein endothelial cells (HUVECs) can contain serotonin (5-HT)-positive WPBs. We show that HUVECs express the vesicular monoamine transporter 1 (VMAT1), and that epitope-tagged VMAT1 localises to WPBs and mediates WPB 5-HT sequestration. Using this new information we applied amperometry, to measure 5-HT release from WPBs. Combining amperometry with high-speed fluorescence imaging of WPB exocytosis in live HUVECs, we have analysed the properties of the WPB fusion pore formed during Ca^{2+} -evoked exocytosis, and the modulation of fusion pore dynamics and WPB exocytosis by depletion or supplementation of cholesterol. Our data highlight an important role for plasma membrane cholesterol in the regulation of WPB exocytosis from endothelial cells.

Results

5-HT is present in WPBs of some HUVECs

Many cells secrete monoamines, which can be detected using amperometry (Chow and Von Ruden, 2009). To examine whether WPBs might contain such molecules we first looked for evidence of endogenous immunoreactivity for the monoamines dopamine, noradrenaline, adrenaline or 5-HT in WPBs. No evidence for WPB dopamine, noradrenaline or adrenaline immunoreactivity was detected; however, we discovered 5-HT immunoreactivity in WPBs in up to 5% of cells (Fig. 1). The relatively low numbers of cells with WPB 5-HT immunoreactivity suggested that electrochemical detection of secreted 5-HT could be problematic. To test this, we applied amperometry to fura-2-loaded HUVECs expressing proregion-EGFP to fluorescently label WPBs. The carbon fibre microelectrode was positioned over regions of the cell containing multiple fluorescent WPBs. Cells were stimulated by gentle mechanical pressure of the electrode on the cell surface, which produced an increase in $[\text{Ca}^{2+}]_i$ and exocytosis of fluorescent WPBs, the kinetics of which are summarised and discussed in supplementary material Fig. S1A. Simultaneous amperometric recording revealed no current spikes associated with exocytosis of fluorescent WPBs under the electrode (supplementary material Fig. S1B), consistent with WPBs in most cells lacking secretable monoamines. Nonetheless, the presence of 5-HT immunoreactivity in some WPBs led us to investigate ways to load WPBs with this monoamine for amperometric analysis of WPB exocytosis.

HUVECs express VMAT1, and EGFP-VMAT1 localises to WPBs resulting in both WPB 5-HT immunoreactivity and current spikes during exocytosis

5-HT immunoreactivity in WPBs suggested the existence of a VMAT on the organelle. RT-PCR of HUVEC cDNA revealed the presence of VMAT1 (encoded by *SLC18A1*) but not VMAT2 (encoded by *SLC18A2*) mRNA. In addition, we found mRNA for the plasma membrane monoamine transporter (PMAT, encoded by *SLC29A4*) but not the serotonin transporter (SERT, encoded by *SLC6A4*) or the organic cation transporter 3 (OCT3, encoded by *SLC22A3*) (supplementary material Fig. S1C). Immunocytochemistry was attempted to establish the subcellular localisation of endogenous VMAT1,

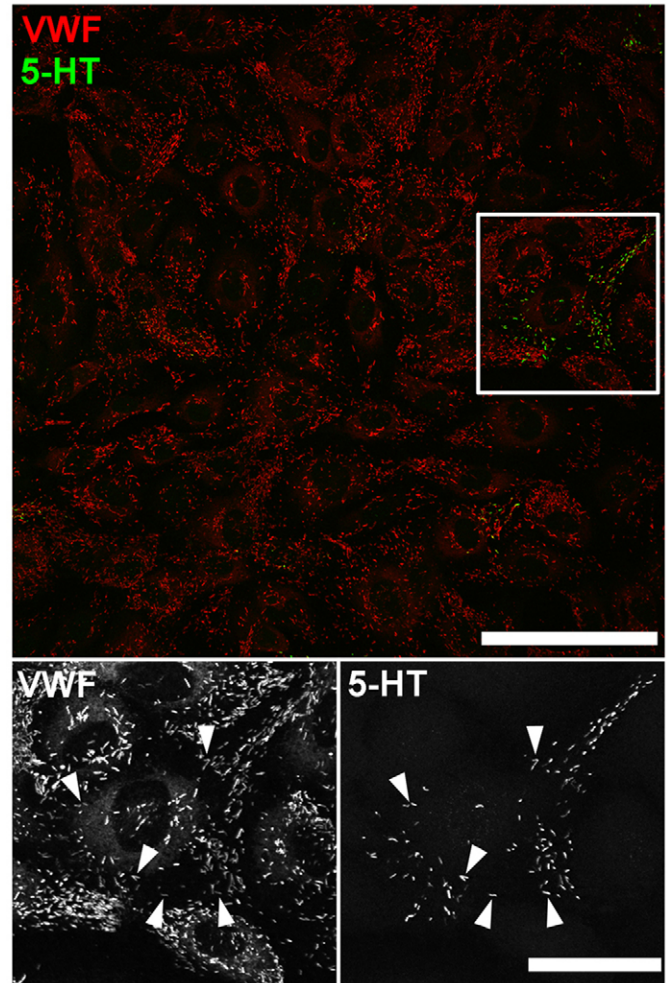


Fig. 1. 5-HT immunoreactivity localises to WPBs in HUVECs. Image shows a field of HUVECs immunolabeled with specific antibodies to VWF (red, rabbit Ab) and 5-HT (green). Scale bar: 100 μm . The region indicated by the white box is shown at an expanded scale in the lower panels. The proportion of cells containing WPB 5-HT immunoreactivity ranged from $0\text{--}5.2 \pm 1.0\%$ [determined from analysis of 48 randomly selected low power ($40\times$ magnification) fields]. Scale bar: 20 μm . Immunofluorescence images of fixed cells shown here and in subsequent figures were taken at room temperature using Leica SP1 or SP2 confocal microscopes and software (Mannheim, Germany) equipped with $40\times$, $63\times$ or $100\times$ objectives (SP1; PL APO40 \times 1.25–0.75 NA, PL APO100 \times 1.4NA, SP2; HCX PL APO40 \times 1.2 NA, PL APO 63 \times 1.4NA, PL APO100 \times 1.4NA).

however, we were unable to detect an endogenous signal with the reagents used. We therefore expressed epitope-tagged VMAT1 to assess the putative subcellular localisation of this VMAT in HUVECs.

EGFP-VMAT1 localised to WPBs, which showed striking WPB 5-HT immunoreactivity (Fig. 2A). No 5-HT immunoreactivity was detected in any other subcellular structures, and the effect was specific for EGFP-VMAT1; expressed EGFP-VChT (vesicular acetylcholine transporter) also localised to WPBs but did not produce WPB 5-HT immunoreactivity (supplementary material Fig. S2A). Consistent with WPB VMAT1 mediating 5-HT sequestration, reserpine treatment abolished WPB 5-HT immunoreactivity in EGFP-VMAT1-expressing cells (supplementary material Fig. S2B).

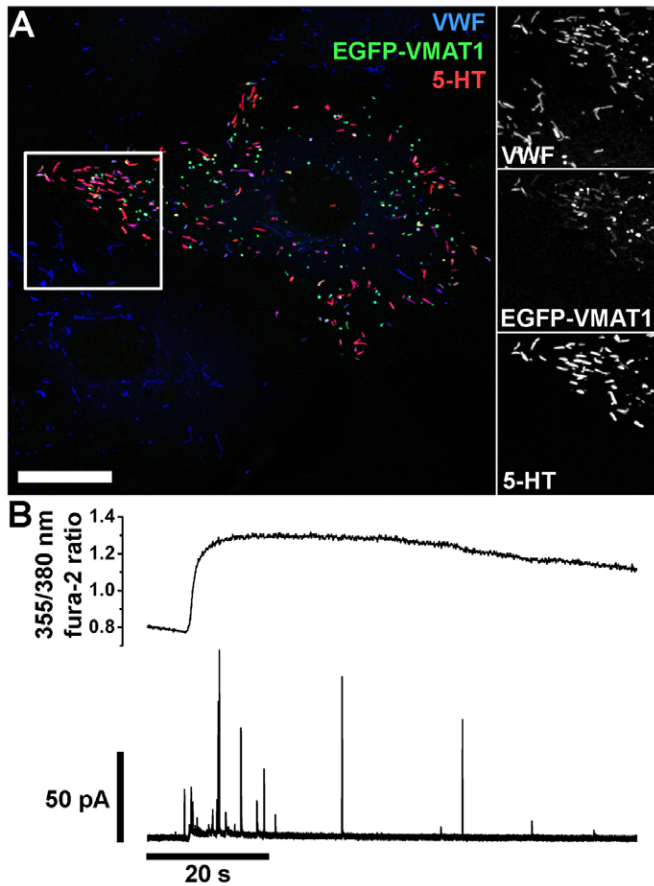


Fig. 2. EGFP-VMAT1 localises to WPBs, and results in the appearance of WPB 5-HT immunoreactivity and current spikes during endothelial cell stimulation. (A) HUVECs expressing EGFP-VMAT1 and immunolabelled with specific antibodies to VWF (blue, rabbit Ab), EGFP (green) and 5-HT (red). Scale bar: 20 μ m. Regions indicated by white boxes are shown in grey scale to the right at an expanded scale. (B) Simultaneous recording of fura-2 fluorescence ratio (top trace) and electrode current (bottom trace) from a single proregion-EGFP- and mCherry-VMAT1-expressing HUVECs following mechanical stimulation with the electrode.

We measured the intra-WPB pH (pH_{WPB}) in epitope-tagged VMAT1-expressing cells, to test whether VMAT1 expression perturbed the pH_{WPB} , but found no differences compared with control cells (supplementary material Fig. S2C). To identify the source of 5-HT in WPBs we focused on the tissue culture fetal calf serum, which is reported to contain up to 7 μM 5-HT (Hamamori et al., 1988; Little et al., 2002; McEwan and Parsons, 1987; Mothersill et al., 2010). 5-HT was first discharged from EGFP-VMAT1-expressing WPBs by exposure to NH_4Cl , after which the cells were incubated in full growth medium, serum-free growth medium or dialysed medium (see Materials and Methods) for 5 hours. In full growth medium WPB 5-HT immunoreactivity was restored; however, in serum-free growth medium or dialysed medium WPB 5-HT immunoreactivity was absent. WPB 5-HT immunoreactivity could be restored by brief exposure to serum-free growth medium or dialysed medium supplemented with $\geq 0.3 \mu\text{M}$ 5-HT. In these cases, WPB 5-HT immunoreactivity remained detectable for up to 16 hours in 5-HT- and serum-free growth medium or dialysed medium (e.g. supplementary material Fig. S3A–C).

Applying amperometry to fura-2-loaded cells coexpressing mCherry-VMAT1 and proregion-mEGFP revealed clear current spikes during cell stimulation (Fig. 2B). Simultaneous optical detection of WPB exocytosis revealed that individual current spikes (Fig. 3A, black trace) were associated with individual WPB fusion events (grey traces). Close inspection revealed a delay between the onset of a current spike and the increase in WPB EGFP fluorescence intensity (Fig. 3B). Spike quantal size (Q) significantly correlated with WPB length (volume) indicating that the concentration of oxidisable species within each individual WPB is similar (supplementary material Fig. S3D). No current spikes were detected in the absence of stimulation, or during stimulation when recording from regions lacking fluorescent WPBs; consistent with current spikes arising solely from WPB exocytotic events.

Properties of current spikes associated with WPB fusion

Fig. 4A shows a typical current spike from a control cell, with each of the measured spike parameters indicated (see also Materials and Methods) and the mean parameter values in parentheses. Pre-spike foot signal parameters are shown in Fig. 4Aii. Current spikes varied in amplitude and shape (Fig. 4B), however, the majority ($74.73 \pm 1.99\%$, $n=68$ cells) showed a clear pre-spike foot signal, often with complex kinetics including ramp-like (Fig. 4Bi), fluctuating (Fig. 4Bii) or more stable plateau-like (Fig. 4Biii) current increases prior to the onset of the fast rise of the main spike. Occasionally, the pre-spike foot signal comprised large amplitude, step-like increases in current (Fig. 4Biv). Fig. 4C shows examples of current spikes lacking pre-spike foot signals. Rarely, small amplitude current increases of variable duration, resembling stand-alone foot signals (Alvarez de Toledo et al., 1993; Chow et al., 1992) were observed (Fig. 4D). In these cases, optical analysis revealed fusion and collapse of the WPB into a spherical structure in which proregion-EGFP was retained (Fig. 4Di, image montage). We next studied the effect of perturbation of total cellular cholesterol on WPB exocytosis, proregion secretion and WPB spike parameters.

Cholesterol modulates WPB exocytosis and fusion pore dynamics

Total cellular cholesterol was reduced or increased by $\sim 50\%$ by treatment with methyl- β -cyclodextrin (M β CD, 5 mM) or cholesterol-loaded M β CD (M β CD-Chol, 5 mM), respectively (Fig. 5A). To confirm that M β CD treatment depleted plasma membrane cholesterol, we immunolabelled M β CD-treated HUVECs with specific antibodies to the caveolae-resident cholesterol-binding protein caveolin-1 (Cav-1). Cholesterol depletion decreases Cav-1 localisation at the plasma membrane and caveolae flatten (Rothberg et al., 1990). Consistent with this there was a reduction in the punctate pattern of plasma membrane Cav-1 immunoreactivity and an increase in the intensity of perinuclear Cav-1 immunoreactivity (Fig. 5Bi,ii), although WPB numbers and morphology were not visibly altered. In M β CD-Chol-treated cells the pattern of Cav-1 immunoreactivity did not appear substantially altered (Fig. 5Biii). Filipin fluorescence intensity was also significantly reduced in M β CD-treated HUVECs, while in M β CD-Chol-treated cells filipin intensity was similar to controls, although its distribution appeared qualitatively altered with reduced intensity at cell–cell contacts (Fig. 5C,D).

Histamine-evoked proregion secretion did not change in M β CD-treated cells, but was significantly increased in M β CD-Chol-treated

cells (Fig. 6Ai,ii). Optical analysis of individual HUVECs showed that histamine-evoked increases in fura-2 fluorescence ratios were similar in control, M β CD- or M β CD-Chol-treated cells, and an averaged record from seven cells is shown in Fig. 6Bi. However, optical analysis did reveal significant differences in the time course of WPB exocytosis between treatment groups, illustrated in the cumulative plots of exocytotic events in Fig. 6Bii. In M β CD-treated cells there was a significant increase in the delay in the onset of exocytosis although rate and the mean fraction of fluorescent

WPBs that underwent exocytosis [a measure of the probability of release, P_r (Bierings et al., 2012)] were not changed (Fig. 6Biii). In M β CD-Chol-treated cells the rate of WPB exocytosis increased significantly (Fig. 6Biii), although delay and P_r were not altered. We next used amperometry to assess the effect of M β CD and M β CD-Chol treatment on the properties of the WPB fusion pore.

WPB spike and pre-spike foot signal parameters recorded from M β CD and M β CD-Chol treated HUVECs are summarised in Fig. 7 (and in supplementary material Table S1C). Cholesterol depletion resulted in a decrease in the spike $t_{1/2}$, t_{rise} and t_{decay} and an increase in the rise rate and I_{max} , as well as a reduction in the duration of the pre-spike foot signal t_{foot} . A trend in the opposite direction was seen after cholesterol supplementation. Overall, data indicate that cholesterol depletion increased the rate of fusion pore expansion and destabilised the early fusion pore whereas cholesterol supplementation had broadly the opposite effect.

Discussion

WPBs accumulate 5-HT through expression of VMAT1

Electrochemical detection of secretion is dependent on the release of electro-active species during exocytosis (Chow and Von Ruden, 2009), such as monoamines, that are stored within secretory granules of neuronal, neuroendocrine and endocrine cells and blood platelets (Eiden et al., 2004). Accumulation of stored monoamines is driven by the electrogenic transporters VMAT1 and/or VMAT2 on the secretory granule membrane (Eiden et al., 2004). To date, there have been no reports that endothelial cells express a VMAT or that WPBs contain monoamines. Here, we show that HUVECs express VMAT1 and that epitope-tagged VMAT1 localises to WPBs and mediates WPB 5-HT sequestration, as indicated by the abolition of WPB 5-HT immunoreactivity by reserpine (or NH₄Cl-mediated neutralisation of the acidic intra-WPB environment). An acidic granule lumen is essential for VMAT function, but also promotes the cationic state of 5-HT, which is both less permeable to the granule membrane and is more likely to bind to anionic proteoglycan matrix components (Marszalek et al., 1997). These contribute to the accumulation of secretory granule 5-HT to a high concentration [up to ~0.5 M (Ge et al., 2009)] and similar processes are likely to occur in WPBs.

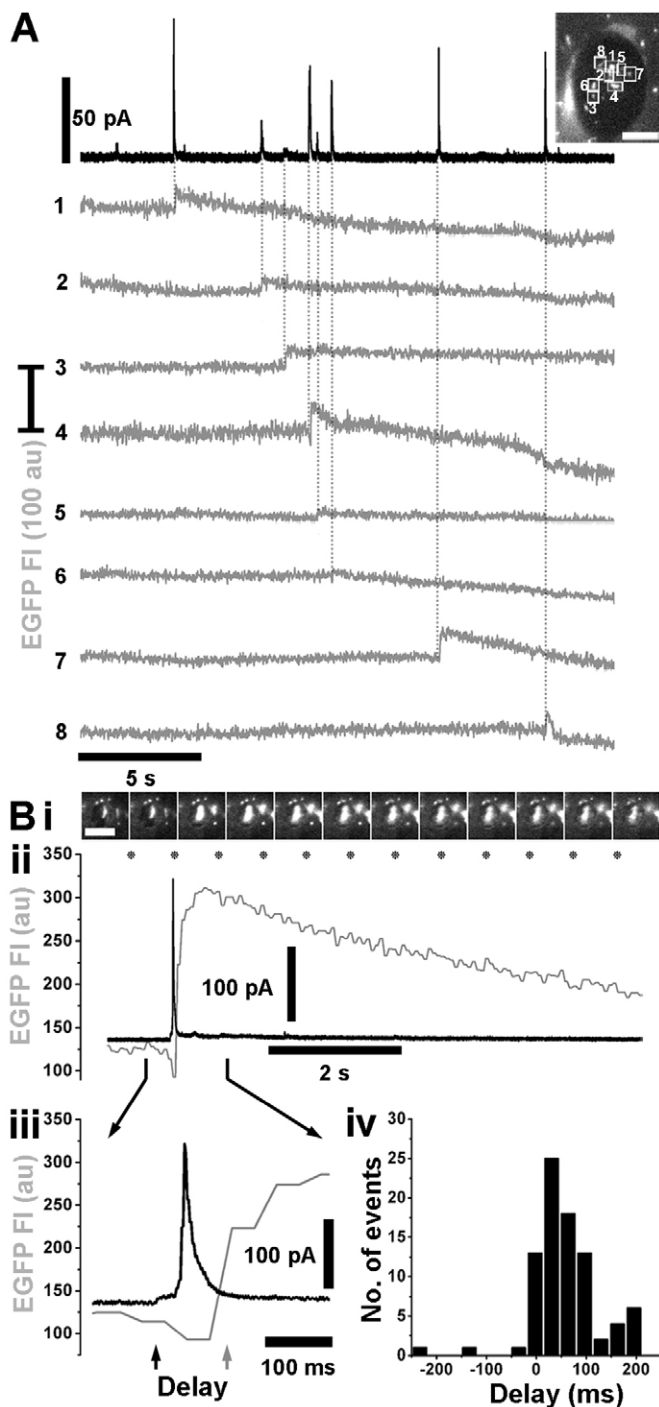


Fig. 3. Current spikes are associated with WPB fusion.

(A) Representative recording of electrode current (black trace) and fluorescence intensity of individual EGFP-labelled WPBs (grey traces, 1–8) in an mCherry–VMAT1 and proregion–EGFP co-expressing HUVEC. Positions of individual EGFP-labelled WPBs (numbered 1–8) beneath the electrode, just prior to stimulation, are shown in the image of the electrode footprint (top right). Scale bar: 5 μ m. A current spike is associated with fusion of each WPB (marked by vertical dotted lines). (Bi) Image montage showing the fusion of a single proregion–EGFP-containing WPB isolated beneath an electrode. Images of EGFP fluorescence were acquired at 15 frames/second, and correspond to the times indicated by the asterisks in Bii. Scale bar: 5 μ m. (Bii–iii) The temporal association between the increase in WPB EGFP fluorescence intensity, due to fusion (grey traces), and the onset of the current spike (black traces). There is a delay between the onset of the current spike (black arrow in Biii) and the onset of the rise in WPB EGFP fluorescence intensity (grey arrow in Biii). (Biv) A summary of the distribution of delay times (bin width, 33 ms; mean 57.4 ± 7.27 ms, $n=84$).

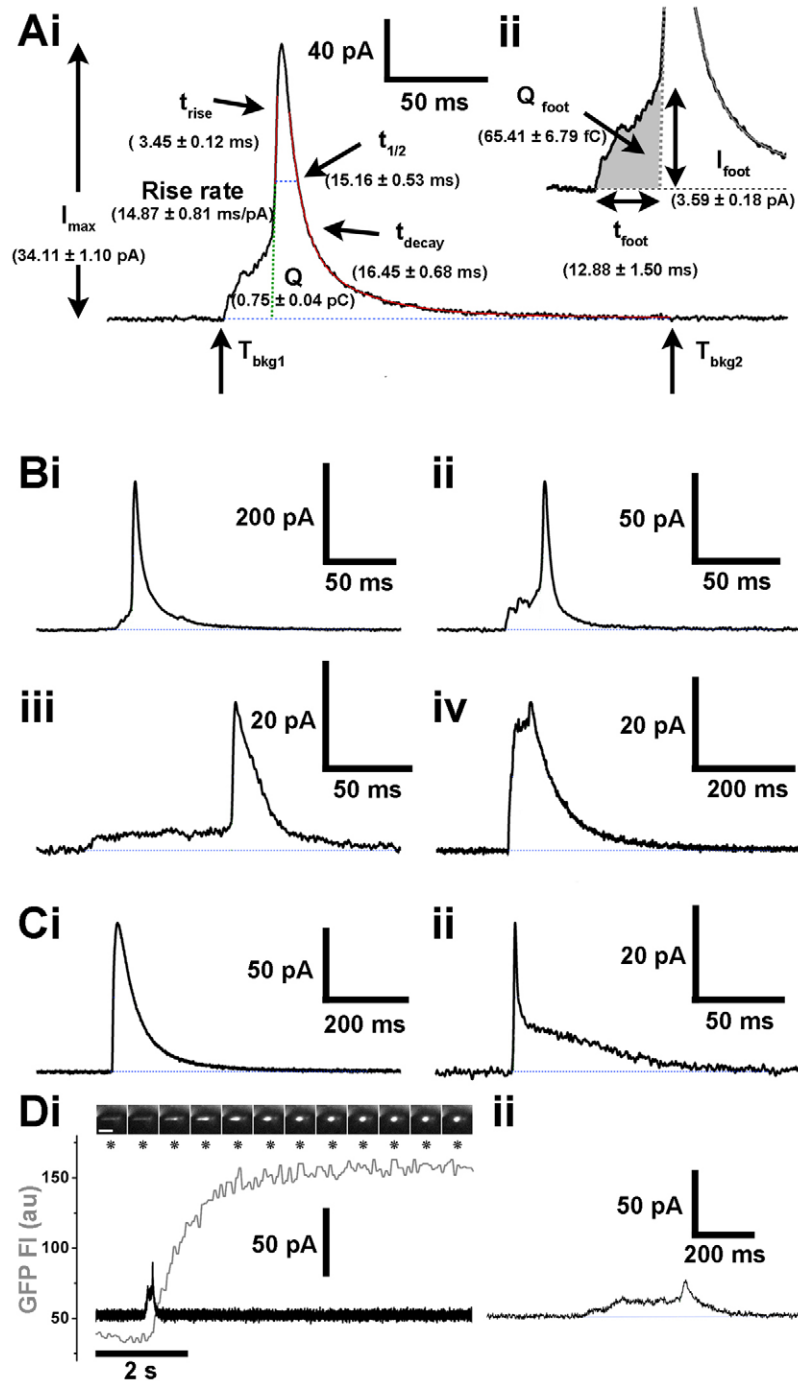


Fig. 4. Electrochemical characterisation of WPB exocytosis – WPBs form a restricted pore prior to full exocytosis.

(Ai) Current spike parameters were calculated between the times when current exceeded five s.d. of the baseline (T_{bkg1}) and subsequently returned to the baseline (T_{bkg2}) and included maximum current amplitude (I_{max}), area (Q), width of the spike at half the amplitude ($t_{1/2}$), duration of the rise (t_{rise}) and decay (t_{decay}) phases between 25% and 75% of the I_{max} and rate of rise (pA/ms). (Aii) Pre-spike foot signal parameters were t_{foot} [which corresponds to the time between T_{bkg1} and the pre-spike foot signal end as defined by the interception of the rise slope with the baseline (Mosharov and Sulzer)], Q_{foot} (shaded area) and I_{foot} [the average current amplitude within t_{foot} (Mosharov and Sulzer, 2005)]. HUVEC parameters (mean \pm s.e.m.) are shown for each in parenthesis ($n=762$ spikes and 542 pre-spike foot signals from 97 cells). (B) WPB current spikes preceded by pre-spike foot signals. Pre-spike foot signals either increased in a ramp-like fashion (i) showed current fluctuations (ii), or showed a plateau phase (iii). Pre-spike foot signals of large amplitude were also observed, resembling a step-like increase prior to the fast phase of the spike (iv). (Ci,ii) Examples of current spikes lacking pre-spike foot signals. (D) Example of a transient WPB fusion event (Babich et al., 2008). (Di) Top panel shows images of the fusion and morphological transition of a single proregion-EGFP containing WPB, isolated beneath the electrode. Images were acquired at 15 frames/second and correspond to the times indicated by the asterisks. Scale bar: 5 μ m. The lower panel shows the time-course for the changes in WPB EGFP fluorescence intensity (grey trace) and current transient (black trace). The current transient is shown on an expanded time scale in Dii.

The source of the 5-HT in WPBs was the tissue culture fetal calf serum. How might extracellular 5-HT enter HUVECs? Pulmonary and brain endothelial cells express SERT (Brust et al., 2000; Ni and Watts, 2006), however, HUVECs appear to lack a high affinity 5-HT uptake mechanism (Mann et al., 1989) and consistent with this we failed to detect SERT mRNA. However, endothelial cells including HUVECs can express low affinity, high capacity monoamine transporters including PMAT and OCT3 (Barnes et al., 2006; Ferik et al., 2012; Solbach et al., 2011). Although we detected PMAT expression (but surprisingly not OCT3), preliminary experiments using the potent PMAT and OCT3 inhibitor decynium-22 (Engel et al., 2004) failed to abolish

WPB 5-HT immunoreactivity, suggesting that 5-HT enters the cell primarily by passive diffusion across the plasma membrane. We failed to detect dopamine, noradrenaline or adrenaline immunoreactivity in WPBs. These monoamines are present in fetal calf serum, but at much lower levels than 5-HT, equivalent to ~ 20 nM for dopamine (Little et al., 2002) and >0.1 nM for noradrenaline or adrenaline (Dibner and Insel, 1981) in full growth medium containing 20% fetal calf serum. The rank order of potency for competitive block of VMAT1-mediated 5-HT transport is 5-HT $>$ dopamine \gg noradrenaline, adrenaline (Erickson et al., 1996), hence it is likely that 5-HT is the predominant WPB monoamine under our tissue culture conditions.

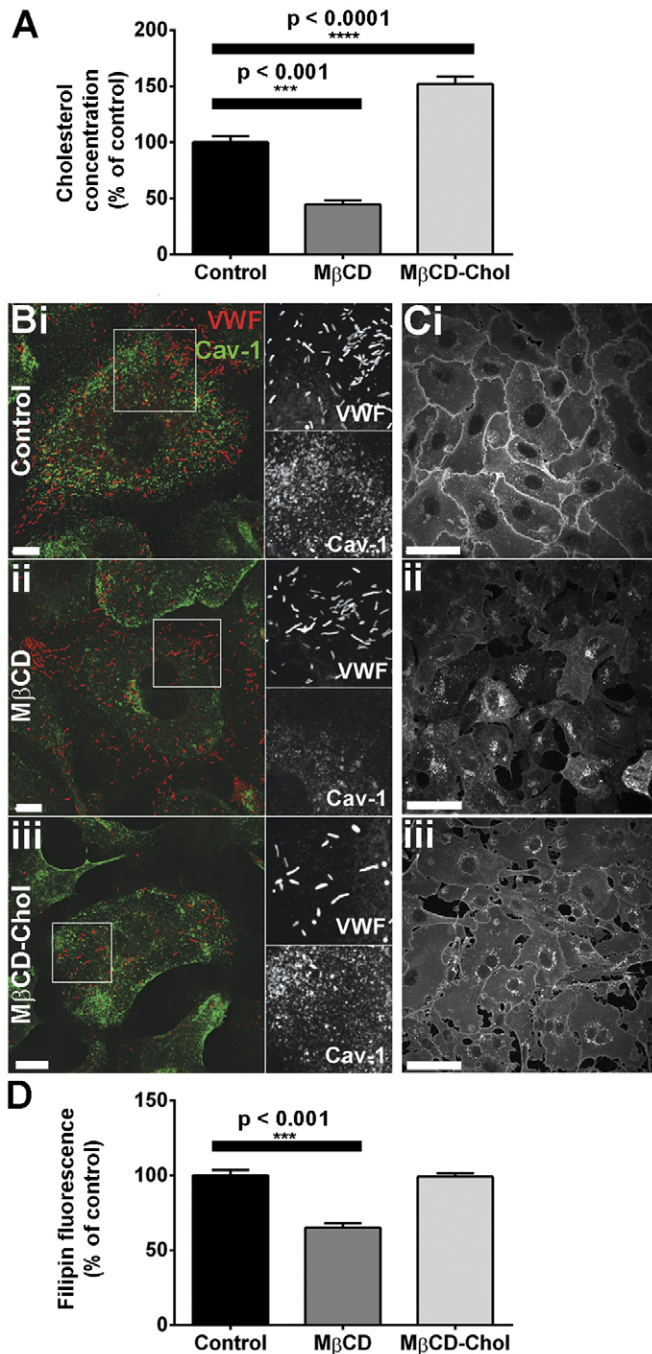


Fig. 5. Depletion or supplementation of HUVEC cholesterol by MβCD. (A) HUVECs were treated with vehicle (control), 5 mM MβCD or 5 mM MβCD-Chol for 30 minutes and cholesterol content was quantified as described in the Materials and Methods. Data were compared by one-way ANOVA ($n=7$ experiments for control, $n=3$ for MβCD and $n=12$ for MβCD-Chol). (B,C) HUVECs treated as described for A were stained with specific antibodies to VWF (red, sheep Ab) and Cav-1 (green) (B) or filipin (C). (D) Filipin fluorescence was quantified for each treatment condition and was compared by one-way ANOVA ($n=75$ cells for control, 80 for MβCD and 120 for MβCD-Chol). Scale bars: 10 μ m (B), 50 μ m (C).

The capacity of some cells to sequester 5-HT in WPBs was not unique to HUVECs; we observed the same in human aortic endothelial cells suggesting a possible physiological relevance.

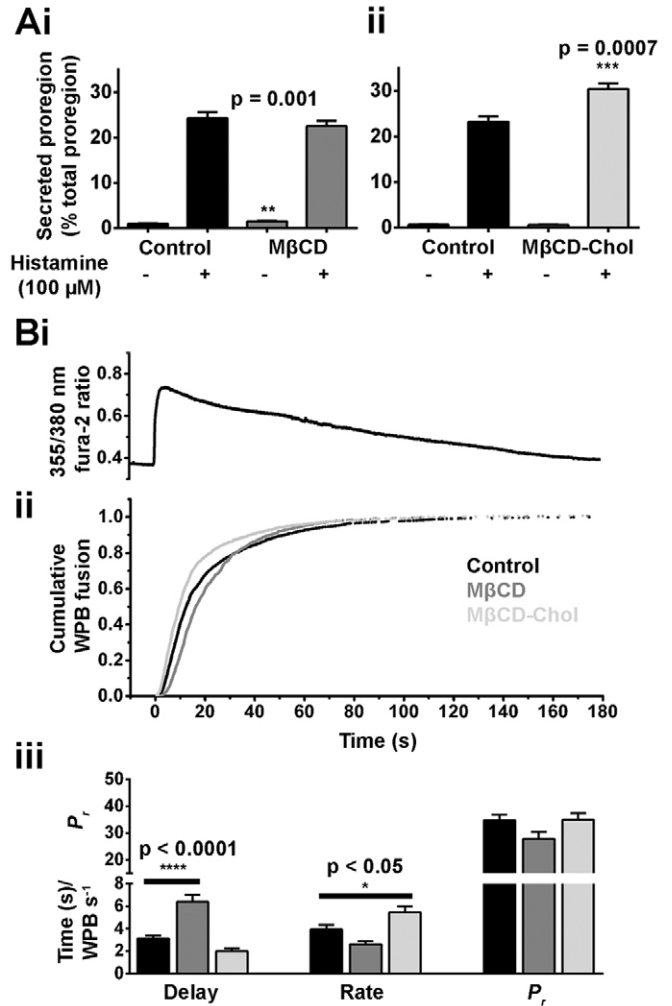
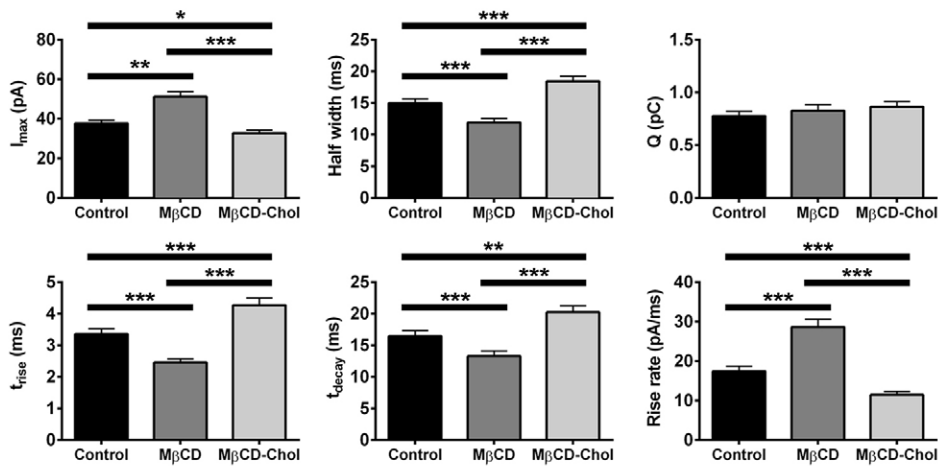


Fig. 6. Perturbation of cellular cholesterol affects hormone-stimulated proregrion secretion and WPB exocytosis. (Ai-ii) Histamine-stimulated secretion of proregrion from HUVECs pre-treated for 30 minutes with vehicle (control), 5 mM MβCD or 5 mM MβCD-Chol. Data were compared by Student's *t*-test ($n=3$ separate experiments for i and ii). (B) Kinetics of histamine-evoked (100 μ M) WPB exocytosis following the same treatment as detailed in A. Increases in fura-2 fluorescence ratios were not different between treatment groups; a trace averaged from seven individual cells is shown in Ai. (ii) Cumulative plots of WPB fusion times, normalised to the total number of fusion events for control (black trace, $n=2057$ events), and cells treated with MβCD (dark grey trace, $n=1101$ events) and MβCD-Chol (light grey trace, $n=2014$ events). (iii) Summary of the mean delay between the $[Ca^{2+}]_i$ rise and first fusion event (seconds), mean maximal rate of exocytosis (WPBs/second) and probability of WPB fusion (P_r , percent, note broken y-axis) for control (black bars, $n=43$ cells), and cells treated with MβCD (dark grey bars, $n=35$ cells) and MβCD-Chol (light grey bars, $n=42$ cells). Data were compared by one-way ANOVA.

Circulating levels of 5-HT are regulated by active 5-HT uptake in platelets (Mercado and Kilic, 2010) and endothelial cells in lung and other organs (Brust et al., 2000; Ni and Watts, 2006). Some endothelial cells (e.g. pulmonary) also make 5-HT (Dempsie and MacLean, 2008), and both receptor-mediated and direct chemical effects of this monoamine are implicated in physiological (e.g. haemostasis) and pathological (e.g. pulmonary hypertension) processes within the vasculature (Berger et al., 2009; Dempsie

Spike parameters



Pre-spike foot signal parameters

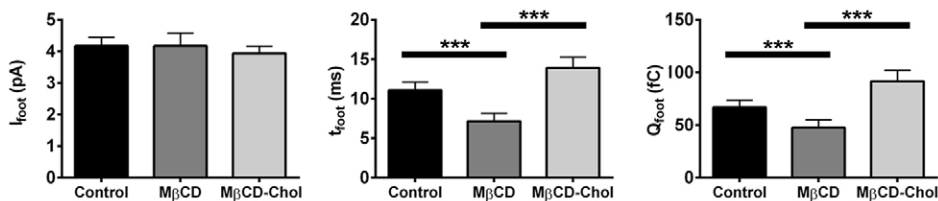


Fig. 7. Cholesterol modulates WPB fusion pore formation and expansion. Top panels show the mean spike parameters in control (black bars, $n=412$ spikes, 51 cells), and cells treated with MβCD (dark grey bars, $n=405$ spikes, 51 cells) and MβCD-Chol (light grey bars, $n=401$ spikes, 51 cells). Bottom panels show the pre-spike foot signal parameters for control (black, $n=303$, 51 cells), and cells treated with MβCD (light grey bars, $n=303$ spikes, 51 cells), and MβCD-Chol ($n=301$, 51 cells).

and MacLean, 2008). The tight regulation of the level of circulating 5-HT is therefore essential. Our observation that WPBs sequester and release 5-HT (and potentially other natural or xenobiotic molecules) provides new insight into this regulation. Storage and release of 5-HT by WPBs could contribute to the control of haemostasis and/or might function as part of a protective mechanism to limit cell damage following exposure to high local concentrations of monoamines (e.g. platelet-derived 5-HT at sites of injury).

Electrochemical analysis of WPB fusion

Current spikes were directly associated with the fusion of individual WPBs. The brief delay between the onset of a current spike and rise in WPB-EGFP fluorescence intensity is probably due to the strong proton buffering of the WPB matrix, estimated at 55 mM pH^{-1} unit (Erent et al., 2007). A striking feature was the high proportion of spikes with a pre-spike foot signal (~75%), showing that the majority of WPB fusions proceed through an initial narrow fusion pore. For comparison, in other cells the typical frequency of spikes with a pre-spike foot signal is much lower, ranging from 5–12% in mast cells (Alvarez de Toledo et al., 1993), 8–11% in platelets (Ge et al., 2009), and up to 20–35% in chromaffin cells (Schroeder et al., 1996). A factor thought to affect the formation of a restricted fusion pore is secretory granule membrane tension; with a low tension increasing the probability of the formation of a restricted fusion pore (Amatore et al., 2005; Ge et al., 2008). WPBs undergo a profound morphological transition during exocytosis, from a cylindrical shape to a sphere (Erent et al., 2007). A sphere has a smaller surface area than a cylinder of the same volume, and so it

is conceivable that for a brief period the WPB membrane tension decreases, favouring the formation of an initially restricted pore. This morphological transition, unique to WPBs, might therefore account for the unusually high proportion of pre-spike foot signals.

Infrequently, we observed current changes reminiscent of stand-alone foot signals, thought to represent the failure of a restricted fusion pore to expand (Fig. 4C), concomitant with WPB fluorescence intensity changes that indicated lingering-kiss fusion (Babich et al., 2008). WPB lingering-kiss fusion was first identified optically and is characterised by the formation of a restricted fusion pore of ~12 nm that does not expand, thereby preventing the release of fluorescent cargo of high molecular mass (Babich et al., 2008). Such events represent ~10% of WPB fusions and are readily detected optically, where most or all fluorescent WPBs can be observed simultaneously. In contrast, the electrode samples only a tiny area of the upper surface of the endothelial cell, reducing the chances of detecting these events. Consequently the characterisation and interpretation of putative stand-alone foot signals was difficult. One feature of such events was a relatively large I_{max} , e.g. 37.31 pA for the example in Fig. 4C, a value within the range of spike amplitudes for full fusion. This probably reflects the large size of the lingering-kiss fusion pore [~12 nm (Babich et al., 2008)], which might not retard 5-HT release substantially. Indeed, a large but not fully expanded pore might account for the unusually large amplitude pre-spike foot signals that we also observed (e.g. Fig. 4Biv). Together, the data indicate that in most cases WPB fusion proceeds through an initial restricted fusion pore, which might 'flicker' reversibly before closing or fully expanding.

Cholesterol modulation of WPB exocytosis

Plasma membrane cholesterol is involved in multiple aspects of exocytosis including organisation of t-SNARE machinery (Churchward and Coorssen, 2009) and modulation of membrane curvature during fusion pore formation (Churchward et al., 2008). Cholesterol depletion inhibits exocytosis in a range of cell types, an effect attributed to the disruption of t-SNARE proteins (Churchward and Coorssen, 2009). We observed a highly significant increase in the delay in the onset of WPB exocytosis (Fig. 6Biii), suggesting that cholesterol depletion might also disrupt t-SNARE proteins in endothelial cells. However, the mean extent of WPB exocytosis (P_r) and proregion secretion was not affected by cholesterol depletion, consistent with a previous study assaying extracellular VWF string formation (Huang et al., 2010). Taken together with reports highlighting the difficulty in blocking VWF secretion by depletion of t-SNARE proteins (Pulido et al., 2011), these results suggest that WPB exocytosis is remarkably resilient to factors that may disrupt plasma membrane composition.

Following cholesterol supplementation, we observed an increase in the rate of WPB exocytosis and the extent of proregion secretion, however, paradoxically not in P_r (although this parameter became more variable). This difference is likely to reflect a small sample size for optical data, compared to biochemical analysis, which assays secretion from millions of cells. These results might also reflect changes in the localisation of t-SNARE proteins; because cholesterol has been implicated in the organisation of fusion sites (Churchward and Coorssen, 2009), supplementation of cholesterol might increase the concentration of t-SNARE proteins allowing increased access of WPBs to plasma membrane fusion machinery.

Cholesterol is also thought to be directly involved in the modulation of the exocytotic fusion pore by stabilising intermediate structures (including the early restricted fusion pore) during bilayer fusion through its ability to promote negative membrane curvature (Chen and Rand, 1997; Churchward and Coorssen, 2009). In agreement with data from platelets, PC12 and chromaffin cells (Ge et al., 2010; Koseoglu et al., 2011; Wang et al., 2010; Zhang et al., 2009), we observed a decrease in pre-spike foot duration following cholesterol depletion, providing further evidence for the role of cholesterol in the formation and stabilisation of the restricted fusion pore. In addition, we observed an increase in the rate of fusion pore expansion, in agreement with data from platelets (Ge et al., 2010) but in contrast to data from PC12 or chromaffin cells (Wang et al., 2010; Zhang et al., 2009). The basis for the discrepancies between different cell types remains unclear.

Our results demonstrate that cholesterol plays multiple roles in WPB exocytosis, influencing the overall extent of exocytosis, and both fusion pore formation and expansion. It is not clear whether acute changes in circulating cholesterol levels substantially impact endothelial cell cholesterol, and one might speculate that endothelial cells are resilient to sudden changes. However, the effects seen here for hormone-evoked WPB exocytosis could reflect an underlying mechanism to account for increased circulating VWF observed together with chronically elevated plasma cholesterol levels (Blann et al., 1995; Pérez-Jiménez et al., 1999) and which contribute to a higher risk of vascular disease (Jansson et al., 1991; Lip and Blann, 1997).

Materials and Methods

Tissue culture, transfections, ELISAs, immunocytochemistry, antibodies, DNA constructs, RT-PCR and reagents

HUVECs were obtained, cultured in full growth medium and transfected as previously described (Bierings et al., 2012). Dialysed medium comprised full

growth medium with 20% dialysed fetal calf serum (24 hours, 4°C, 0.15 M NaCl, 10,000 MWCO SnakeSkin tubing; Thermo Fisher Scientific, Cramlington, UK). Serum-free growth medium was supplemented with 20 mM HEPES (pH 7.4) and 2% BSA. Immunocytochemistry and ELISAs for the proregion were performed as previously described (Bierings et al., 2012). Sources and dilutions of all antibodies used are in supplementary material Table S1A. Proregion-mEGFP and P-selectin-mCherry were made as previously described (Bierings et al., 2012 and references therein). EGFP-VMAT1 (Essand et al., 2005) was provided by Professor Giandomenico (University of Uppsala, Sweden). mCherry-VMAT1 was made by exchanging EGFP with mCherry as an *NheI/BsrGI* fragment cut from pmCherry-C2 (Clontech, Mountain View, CA) and cloned into *NheI/BsrGI* digested EGFP-VMAT1. EGFP-VAcHT was from Professor Takahashi (Department of Biochemistry, Kitasato-University School of Medicine, Japan). RNA was extracted from HUVECs, BON cells or human adrenal tissue (from Medical Solutions Plc, Nottingham, UK, used in accordance with the terms of the MRC NIMR Human Tissue Authority licence) as previously described (Bierings et al., 2012). RT-PCR was performed using the SuperScript III Reverse Transcriptase kit (Invitrogen, Grand Island, NY, USA). Primer sequences for PMAT, VMAT1, VMAT2, SERT and OCT3 are in supplementary material Table S1B. Fura-2 AM was from Molecular Probes (Eugene, OR, USA). Other reagents were from Sigma-Aldrich (Gillingham, UK) unless otherwise stated.

Determining the source of WPB-associated 5-HT

Non-transfected or EGFP-VMAT1-expressing HUVECs (16 or 48 hours post-transfection) were exposed to vehicle or 10 mM NH_4Cl for 5 minutes in serum-free growth medium, followed by incubation in dialysed medium or serum-free growth medium for 5 to 16 hours in the absence or presence of 5-HT (0.03–3 μM) prior to immunocytochemistry.

Cholesterol depletion and supplementation

Non-transfected, proregion-EGFP-, or proregion-EGFP- and mCherry-VMAT1-expressing HUVECs (48 hours post-transfection) were exposed to vehicle (distilled H_2O), 5 mM M β CD or 5 mM M β CD-Chol in serum-free growth medium for 30 minutes. M β CD-Chol was made as previously described (Klein et al., 1995). Filipin (10 $\mu\text{g/ml}$) staining was performed on fixed cells as for immunocytochemistry (Bierings et al., 2012). Total cellular cholesterol was quantified using an Amplex Red cholesterol assay kit according to the manufacturer's instructions (Invitrogen, Grand Island, NY, USA) using a microplate reader (Molecular Devices Corporation, Sunnyvale, CA, USA).

Live-cell fluorescence imaging and intra-WPB pH measurements

Imaging of fura-2, proregion-EGFP-containing WPBs and measurements of intra-WPB pH were carried out using both total internal reflection fluorescence (TIRF) and epifluorescence microscopy as described previously (Erent et al., 2007). The mean fraction of fluorescent WPBs that underwent exocytosis was taken as a measure of the probability of release, P_r , as previously described (Bierings et al., 2012). Images were acquired at 30–100 frames/second, image capture was synchronised with illumination using Winfluor software (<http://spider.science.strath.ac.uk>).

Carbon fibre microelectrode fabrication, preparation and amperometric recording

Electrodes were fabricated as described in Pike et al. (Pike et al., 2009). Electrodes were sealed with epoxy resin (~90°C), cured overnight at room temperature and then baked at 100°C for 2 hours and 150°C for ~24 hours. This was repeated but with an extended curing period of 2–5 days at 150°C. Electrode tips were bevelled to 45° on a microelectrode beveller with a coarse diamond abrasive plate (Sutter Instruments, Novato, CA) and soaked in 2-propanol for ~20 minutes. Electrodes were tested as previously described (Schulte and Chow, 1996) and those with a stable baseline current used. Electrodes were re-bevelled after 1–3 experiments. Electrodes were backfilled with 150 mM KCl solution and connected to an Axopatch 200B amplifier (Axon Instruments, Foster City, CA, USA) in voltage clamp configuration, and held at +700 mV versus a silver/silver chloride reference electrode, for detection of 5-HT, dopamine, noradrenaline and adrenaline. Data were acquired at 10 KHz, filtered at 5 KHz, and recorded using Winfluor software. Prior to amperometry, cells co-expressing mCherry-VMAT1 and proregion-EGFP (48 hours post transfection) were exposed to 100 μM 5-HT in serum-free growth medium, to enhance WPB-5-HT loading. Cells were fura-2-loaded as previously described (Erent et al., 2007). Stimulation was by gentle mechanical pressure of the electrode onto the cell. Fura-2 355 nm fluorescence was monitored to determine if stimulation caused cell rupture (indicated by a quench in 355 nm fluorescence), however this was not seen to occur.

Data analysis

Amperometric data were analysed using a custom written macro for Igor Pro (Mosharov and Sulzer, 2005) (<http://www.sulzerlab.org/download.html>). Traces were low-pass filtered (1000 Hz Gaussian filter) followed by binomial smoothing (500 Hz). Thresholds for spike and foot detection were five and two times the

root-mean-square of the background current, respectively. Spike parameters determined included: I_{\max} , maximum spike amplitude; Q , integrated spike charge; $t_{1/2}$, spike width at half the spike maximum; t_{rise} , 25–75% rise time of the spike; rise slope, rate of the rising phase of the spike; and t_{decay} , duration of the decay phase of the spike between 75 and 25% of the amplitude. Pre-spike foot signal parameters were: I_{foot} , average amplitude; t_{foot} , duration and Q_{foot} , integrated charge. Spikes with a t_{rise} greater than 3 s.d. + mean t_{rise} were rejected, as previously described (Mosharov and Sulzer, 2005). Statistical analysis and comparison of log-transformed current spike parameters was carried out by one-way ANOVA, with a Bonferroni post test to compare pairs of data sets, and for secretion data by Student's *t*-test or one-way ANOVA as indicated, in GraphPad Prism Version 5 (GraphPad Software Inc., La Jolla, USA). Image analysis was carried out in WinFluor software or using custom-written plugins and macros in ImageJ software (<http://rsb.info.nih.gov/ij/>) as previously described (Bierings et al., 2012; Erent et al., 2007). Data were plotted in Microcal Origin 8 (OriginLab Corp., Northampton, MA, USA). Data are expressed as mean \pm s.e.m.

Author contributions

E.A.C. I.L.C. M.J.H. and T.C. performed research and analyzed data; J.D. contributed vital tools; E.A.C. I.L.C. M.J.H. and T.C. designed the research and wrote the paper.

Funding

The work was supported by the UK Medical Research Council [grant number U117573808 to T.C.]. Deposited in PMC for immediate release.

Supplementary material available online at

<http://jcs.biologists.org/lookup/suppl/doi:10.1242/jcs.138438/-DC1>

References

- Alvarez de Toledo, G., Fernández-Chacón, R. and Fernández, J. M. (1993). Release of secretory products during transient vesicle fusion. *Nature* **363**, 554–558.
- Amatore, C., Arbault, S., Bonifas, I., Bouret, Y., Erard, M., Ewing, A. G. and Sompers, L. A. (2005). Correlation between vesicle quantal size and fusion pore release in chromaffin cell exocytosis. *Biophys. J.* **88**, 4411–4420.
- Anantharam, A., Bittner, M. A., Aikman, R. L., Stuenkel, E. L., Schmid, S. L., Axelrod, D. and Holz, R. W. (2011). A new role for the dynamin GTPase in the regulation of fusion pore expansion. *Mol. Biol. Cell* **22**, 1907–1918.
- Babich, V., Meli, A., Knipe, L., Dempster, J. E., Skehel, P., Hannah, M. J. and Carter, T. (2008). Selective release of molecules from Weibel-Palade bodies during a lingering kiss. *Blood* **111**, 5282–5290.
- Barnes, K., Dobrzynski, H., Foppolo, S., Beal, P. R., Ismat, F., Scullion, E. R., Sun, L., Tellez, J., Ritzel, M. W., Claycomb, W. C. et al. (2006). Distribution and functional characterization of equilibrative nucleoside transporter-4, a novel cardiac adenosine transporter activated at acidic pH. *Circ. Res.* **99**, 510–519.
- Berberian, K., Torres, A. J., Fang, Q., Kisler, K. and Lindau, M. (2009). F-actin and myosin II accelerate catecholamine release from chromaffin granules. *J. Neurosci.* **29**, 863–870.
- Berger, M., Gray, J. A. and Roth, B. L. (2009). The expanded biology of serotonin. *Annu. Rev. Med.* **60**, 355–366.
- Bierings, R., Hellen, N., Kiskin, N., Knipe, L., Fonseca, A. V., Patel, B., Meli, A., Rose, M., Hannah, M. J. and Carter, T. (2012). The interplay between the Rab27A effectors Slp4-a and MyRIP controls hormone-evoked Weibel-Palade body exocytosis. *Blood* **120**, 2757–2767.
- Blann, A. D., Jackson, P., Bath, P. M. and Watts, G. F. (1995). von Willebrand factor, a possible indicator of endothelial cell damage, decreases during long-term compliance with a lipid-lowering diet. *J. Intern. Med.* **237**, 557–561.
- Braun, M., Wendt, A., Karanaukaite, J., Galvanovskis, J., Clark, A., MacDonald, P. E. and Rorsman, P. (2007). Corelease and differential exit via the fusion pore of GABA, serotonin, and ATP from LDCV in rat pancreatic beta cells. *J. Gen. Physiol.* **129**, 221–231.
- Brust, P., Friedrich, A., Krizbai, I. A., Bergmann, R., Roux, F., Ganapathy, V. and Johannsen, B. (2000). Functional expression of the serotonin transporter in immortalized rat brain microvessel endothelial cells. *J. Neurochem.* **74**, 1241–1248.
- Chang, J., Kim, S. A., Lu, X., Su, Z., Kim, S. K. and Shin, Y. K. (2009). Fusion step-specific influence of cholesterol on SNARE-mediated membrane fusion. *Biophys. J.* **96**, 1839–1846.
- Chen, Z. and Rand, R. P. (1997). The influence of cholesterol on phospholipid membrane curvature and bending elasticity. *Biophys. J.* **73**, 267–276.
- Chow, R. H. and Von Ruden, L. (2009). Electrochemical detection of secretion from single cells. In *Single-Channel Recording* (ed. B. Sakmann and E. Neher). New York, NY: Springer.
- Chow, R. H., von Rüden, L. and Neher, E. (1992). Delay in vesicle fusion revealed by electrochemical monitoring of single secretory events in adrenal chromaffin cells. *Nature* **356**, 60–63.
- Churchward, M. A. and Coorsen, J. R. (2009). Cholesterol, regulated exocytosis and the physiological fusion machine. *Biochem. J.* **423**, 1–14.
- Churchward, M. A., Rogasevskaia, T., Brandman, D. M., Khosravani, H., Nava, P., Atkinson, J. K. and Coorsen, J. R. (2008). Specific lipids supply critical negative spontaneous curvature—an essential component of native Ca^{2+} -triggered membrane fusion. *Biophys. J.* **94**, 3976–3986.
- Demer, L. L., Wortham, C. M., Dirksen, E. R. and Sanderson, M. J. (1993). Mechanical stimulation induces intercellular calcium signaling in bovine aortic endothelial cells. *Am. J. Physiol.* **264**, H2094–H2102.
- Dempsey, Y. and MacLean, M. R. (2008). Pulmonary hypertension: therapeutic targets within the serotonin system. *Br. J. Pharmacol.* **155**, 455–462.
- Diamond, S. L., Sachs, F. and Sigurdson, W. J. (1994). Mechanically induced calcium mobilization in cultured endothelial cells is dependent on actin and phospholipase. *Arterioscler. Thromb.* **14**, 2000–2006.
- Dibner, M. D. and Insel, P. A. (1981). Serum catecholamines desensitize beta-adrenergic receptors of cultured C6 glioma cells. *J. Biol. Chem.* **256**, 7343–7346.
- Eiden, L. E., Schäfer, M. K., Weihe, E. and Schütz, B. (2004). The vesicular amine transporter family (SLC18): amine/proton antiporters required for vesicular accumulation and regulated exocytotic secretion of monoamines and acetylcholine. *Pflugers Arch.* **447**, 636–640.
- Engel, K., Zhou, M. and Wang, J. (2004). Identification and characterization of a novel monoamine transporter in the human brain. *J. Biol. Chem.* **279**, 50042–50049.
- Erent, M., Meli, A., Moiso, N., Babich, V., Hannah, M. J., Skehel, P., Knipe, L., Zupancic, G., Ogden, D. and Carter, T. (2007). Rate, extent and concentration dependence of histamine-evoked Weibel-Palade body exocytosis determined from individual fusion events in human endothelial cells. *J. Physiol.* **583**, 195–212.
- Erickson, J. D., Schafer, M. K., Bonner, T. I., Eiden, L. E. and Weihe, E. (1996). Distinct pharmacological properties and distribution in neurons and endocrine cells of two isoforms of the human vesicular monoamine transporter. *Proc. Natl. Acad. Sci. USA* **93**, 5166–5171.
- Essand, M., Vikman, S., Grawé, J., Gedda, L., Hellberg, C., Oberg, K., Totterman, T. H. and Giandomenico, V. (2005). Identification and characterization of a novel splicing variant of vesicular monoamine transporter 1. *J. Mol. Endocrinol.* **35**, 489–501.
- Fang, Q., Berberian, K., Gong, L. W., Hafez, I., Sørensen, J. B. and Lindau, M. (2008). The role of the C terminus of the SNARE protein SNAP-25 in fusion pore opening and a model for fusion pore mechanics. *Proc. Natl. Acad. Sci. USA* **105**, 15388–15392.
- Ferk, P., Lipnik-Štangelj, M., Kržan, M. and Černe, K. (2012). Expression of organic cation transporter 3 (SLC22A3) and plasma membrane monoamine transporter (SLC29A4) in human umbilical vein endothelial cells and their relevance for histamine uptake. *BMC Pharmacol. Toxicol.* **13**, Suppl. 1, A73.
- Finnegan, J. M., Pihel, K., Cahill, P. S., Huang, L., Zerby, S. E., Ewing, A. G., Kennedy, R. T. and Wightman, R. M. (1996). Vesicular quantal size measured by amperometry at chromaffin, mast, pheochromocytoma, and pancreatic beta-cells. *J. Neurochem.* **66**, 1914–1923.
- Fu, J., Naren, A. P., Gao, X., Ahmed, G. U. and Malik, A. B. (2005). Protease-activated receptor-1 activation of endothelial cells induces protein kinase Alpha-dependent phosphorylation of syntaxin 4 and Munc18c: role in signaling p-selectin expression. *J. Biol. Chem.* **280**, 3178–3184.
- Galbusera, M., Zoja, C., Donadelli, R., Paris, S., Morigi, M., Benigni, A., Figliuzzi, M., Remuzzi, G. and Remuzzi, A. (1997). Fluid shear stress modulates von Willebrand factor release from human vascular endothelium. *Blood* **90**, 1558–1564.
- Ge, S., Wittenberg, N. J. and Haynes, C. L. (2008). Quantitative and real-time detection of secretion of chemical messengers from individual platelets. *Biochemistry* **47**, 7020–7024.
- Ge, S., White, J. G. and Haynes, C. L. (2009). Quantal release of serotonin from platelets. *Anal. Chem.* **81**, 2935–2943.
- Ge, S., White, J. G. and Haynes, C. L. (2010). Critical role of membrane cholesterol in exocytosis revealed by single platelet study. *ACS Chem. Biol.* **5**, 819–828.
- Goligorsky, M. S. (1988). Mechanical stimulation induces Ca^{2+} transients and membrane depolarization in cultured endothelial cells. Effects on Ca^{2+} in co-perfused smooth muscle cells. *FEBS Lett.* **240**, 59–64.
- Hamamori, Y., Hoshijima, M., Ohmori, T., Ueda, T. and Takai, Y. (1988). Serotonin as a major serum factor inducing the phospholipase C-mediated hydrolysis of phosphoinositides in normal rat kidney cells. *Cancer Res.* **48**, 6697–6702.
- Hewlett, L., Zupančič, G., Mashanov, G., Knipe, L., Ogden, D., Hannah, M. J. and Carter, T. (2011). Temperature-dependence of Weibel-Palade body exocytosis and cell surface dispersal of von Willebrand factor and its propolypeptide. *PLoS ONE* **6**, e27314.
- Huang, J., Motto, D. G., Bundle, D. R. and Sadler, J. E. (2010). Shiga toxin B subunits induce VWF secretion by human endothelial cells and thrombotic microangiopathy in ADAMTS13-deficient mice. *Blood* **116**, 3653–3659.
- Jackson, M. B. and Chapman, E. R. (2008). The fusion pores of Ca^{2+} -triggered exocytosis. *Nat. Struct. Mol. Biol.* **15**, 684–689.
- Jansson, J. H., Nilsson, T. K. and Johnson, O. (1991). von Willebrand factor in plasma: a novel risk factor for recurrent myocardial infarction and death. *Br. Heart J.* **66**, 351–355.
- Klein, U., Gimpl, G. and Fahrenholz, F. (1995). Alteration of the myometrial plasma membrane cholesterol content with beta-cyclodextrin modulates the binding affinity of the oxytocin receptor. *Biochemistry* **34**, 13784–13793.
- Knipe, L., Meli, A., Hewlett, L., Bierings, R., Dempster, J., Skehel, P., Hannah, M. J. and Carter, T. (2010). A revised model for the secretion of tPA and cytokines from cultured endothelial cells. *Blood* **116**, 2183–2191.

- König, J., Prenen, J., Nilius, B. and Gerke, V. (1998). The annexin II-p11 complex is involved in regulated exocytosis in bovine pulmonary artery endothelial cells. *J. Biol. Chem.* **273**, 19679-19684.
- Koseoglu, S., Love, S. A. and Haynes, C. L. (2011). Cholesterol effects on vesicle pools in chromaffin cells revealed by carbon-fiber microelectrode amperometry. *Anal. Bioanal. Chem.* **400**, 2963-2971.
- Lip, G. Y. and Blann, A. (1997). von Willebrand factor: a marker of endothelial dysfunction in vascular disorders? *Cardiovasc. Res.* **34**, 255-265.
- Little, K. Y., Elmer, L. W., Zhong, H., Scheys, J. O. and Zhang, L. (2002). Cocaine induction of dopamine transporter trafficking to the plasma membrane. *Mol. Pharmacol.* **61**, 436-445.
- Mann, G. E., Pearson, J. D., Sheriff, C. J. and Toothill, V. J. (1989). Expression of amino acid transport systems in cultured human umbilical vein endothelial cells. *J. Physiol.* **410**, 325-339.
- Marszalek, P. E., Farrell, B., Verdugo, P. and Fernandez, J. M. (1997). Kinetics of release of serotonin from isolated secretory granules. II. Ion exchange determines the diffusivity of serotonin. *Biophys. J.* **73**, 1169-1183.
- McEwan, M. and Parsons, P. G. (1987). Inhibition of melanization in human melanoma cells by a serotonin uptake inhibitor. *J. Invest. Dermatol.* **89**, 82-86.
- Mendoza, S. A., Fang, J., Gutterman, D. D., Wilcox, D. A., Bubolz, A. H., Li, R., Suzuki, M. and Zhang, D. X. (2010). TRPV4-mediated endothelial Ca²⁺ influx and vasodilation in response to shear stress. *Am. J. Physiol.* **298**, H466-H476.
- Mercado, C. P. and Kilic, F. (2010). Molecular mechanisms of SERT in platelets: regulation of plasma serotonin levels. *Mol. Interv.* **10**, 231-241.
- Mosharov, E. V. and Sulzer, D. (2005). Analysis of exocytotic events recorded by amperometry. *Nat. Methods* **2**, 651-658.
- Mothersill, C., Saroya, R., Smith, R. W., Singh, H. and Seymour, C. B. (2010). Serum serotonin levels determine the magnitude and type of bystander effects in medium transfer experiments. *Radiat. Res.* **174**, 119-123.
- Neco, P., Fernández-Peruchena, C., Navas, S., Gutiérrez, L. M., de Toledo, G. A. and Alés, E. (2008). Myosin II contributes to fusion pore expansion during exocytosis. *J. Biol. Chem.* **283**, 10949-10957.
- Ni, W. and Watts, S. W. (2006). 5-hydroxytryptamine in the cardiovascular system: focus on the serotonin transporter (SERT). *Clin. Exp. Pharmacol. Physiol.* **33**, 575-583.
- Nightingale, T. D., Pattni, K., Hume, A. N., Seabra, M. C. and Cutler, D. F. (2009). Rab27a and MyRIP regulate the amount and multimeric state of VWF released from endothelial cells. *Blood* **113**, 5010-5018.
- Nilius, B., Droogmans, G. and Wondergem, R. (2003). Transient receptor potential channels in endothelium: solving the calcium entry puzzle? *Endothelium* **10**, 5-15.
- Obermüller, S., Lindqvist, A., Karanaukaite, J., Galvanovskis, J., Rorsman, P. and Barg, S. (2005). Selective nucleotide-release from dense-core granules in insulin-secreting cells. *J. Cell Sci.* **118**, 4271-4282.
- Pérez-Jiménez, F., Castro, P., López-Miranda, J., Paz-Rojas, E., Blanco, A., López-Segura, F., Velasco, F., Marín, C., Fuentes, F. and Ordovás, J. M. (1999). Circulating levels of endothelial function are modulated by dietary monounsaturated fat. *Atherosclerosis* **145**, 351-358.
- Pike, C. M., Grabner, C. P. and Harkins, A. B. (2009). Fabrication of amperometric electrodes. *J. Vis. Exp.* **27**, e1040.
- Pulido, I. R., Jahn, R. and Gerke, V. (2011). VAMP3 is associated with endothelial weibel-palade bodies and participates in their Ca²⁺-dependent exocytosis. *Biochim. Biophys. Acta* **1813**, 1038-1044.
- Qizilbash, N., Duffy, S., Prentice, C. R., Boothby, M. and Warlow, C. (1997). Von Willebrand factor and risk of ischemic stroke. *Neurology* **49**, 1552-1556.
- Rojo Pulido, I., Nightingale, T. D., Darchen, F., Seabra, M. C., Cutler, D. F. and Gerke, V. (2011). Myosin Va acts in concert with Rab27a and MyRIP to regulate acute von-Willebrand factor release from endothelial cells. *Traffic* **12**, 1371-1382.
- Rondaij, M. G., Bierings, R., Kragt, A., van Mourik, J. A. and Voorberg, J. (2006). Dynamics and plasticity of Weibel-Palade bodies in endothelial cells. *Arterioscler. Thromb. Vasc. Biol.* **26**, 1002-1007.
- Rothberg, K. G., Ying, Y. S., Kamen, B. A. and Anderson, R. G. (1990). Cholesterol controls the clustering of the glycosphospholipid-anchored membrane receptor for 5-methyltetrahydrofolate. *J. Cell Biol.* **111**, 2931-2938.
- Sadler, J. E. (1998). Biochemistry and genetics of von Willebrand factor. *Annu. Rev. Biochem.* **67**, 395-424.
- Schroeder, T. J., Borges, R., Finnegan, J. M., Pihel, K., Amatore, C. and Wightman, R. M. (1996). Temporally resolved, independent stages of individual exocytotic secretion events. *Biophys. J.* **70**, 1061-1068.
- Schulte, A. and Chow, R. H. (1996). A simple method for insulating carbon-fiber microelectrodes using anodic electrophoretic deposition of paint. *Anal. Chem.* **68**, 3054-3058.
- Segovia, M., Alés, E., Montes, M. A., Bonifas, I., Jemal, I., Lindau, M., Maximov, A., Südhof, T. C. and Alvarez de Toledo, G. (2010). Push-and-pull regulation of the fusion pore by synaptotagmin-7. *Proc. Natl. Acad. Sci. USA* **107**, 19032-19037.
- Sigurdson, W. J., Sachs, F. and Diamond, S. L. (1993). Mechanical perturbation of cultured human endothelial cells causes rapid increases of intracellular calcium. *Am. J. Physiol.* **264**, H1745-H1752.
- Soekmadji, C. and Thorn, P. (2010). Secretory control: evidence for agonist regulation of post-fusion vesicle behaviour. *Clin. Exp. Pharmacol. Physiol.* **37**, 218-221.
- Solbach, T. F., Grube, M., Fromm, M. F. and Zolk, O. (2011). Organic cation transporter 3: expression in failing and nonfailing human heart and functional characterization. *J. Cardiovasc. Pharmacol.* **58**, 409-417.
- Springer, T. A. (2011). Biology and physics of von Willebrand factor concatamers. *J. Thromb. Haemost.* **9 Suppl.** **1**, 130-143.
- Starke, R. D., Ferraro, F., Paschalaki, K. E., Dryden, N. H., McKinnon, T. A., Sutton, R. E., Payne, E. M., Haskard, D. O., Hughes, A. D., Cutler, D. F. et al. (2011). Endothelial von Willebrand factor regulates angiogenesis. *Blood* **117**, 1071-1080.
- Terraube, V., Marx, I. and Denis, C. V. (2007). Role of von Willebrand factor in tumor metastasis. *Thromb. Res.* **120 Suppl.** **2**, S64-S70.
- van Breevoort, D., van Agtmaal, E. L., Dragt, B. S., Gebbinck, J. K., Dienava-Verdoold, L., Kragt, A., Bierings, R., Horrevoets, A. J., Valentijn, K. M., Eikenboom, J. C. et al. (2012). Proteomic screen identifies IGFBP7 as a novel component of endothelial cell-specific Weibel-Palade bodies. *J. Proteome Res.* **11**, 2925-2936.
- Vardjan, N., Stenovec, M., Jorgacevski, J., Kreft, M. and Zorec, R. (2007). Subnanometer fusion pores in spontaneous exocytosis of peptidergic vesicles. *J. Neurosci.* **27**, 4737-4746.
- Vardjan, N., Stenovec, M., Jorgacevski, J., Kreft, M., Grilc, S. and Zorec, R. (2009). The fusion pore and vesicle cargo discharge modulation. *Ann. N. Y. Acad. Sci.* **1152**, 135-144.
- Wagner, D. D. (1990). Cell biology of von Willebrand factor. *Annu. Rev. Cell Biol.* **6**, 217-242.
- Wang, N., Kwan, C., Gong, X., de Chaves, E. P., Tse, A. and Tse, F. W. (2010). Influence of cholesterol on catecholamine release from the fusion pore of large dense core chromaffin granules. *J. Neurosci.* **30**, 3904-3911.
- Zhang, J., Xue, R., Ong, W. Y. and Chen, P. (2009). Roles of cholesterol in vesicle fusion and motion. *Biophys. J.* **97**, 1371-1380.
- Zimmerberg, J. and Chernomordik, L. V. (2005). Neuroscience. Synaptic membranes bend to the will of a neurotoxin. *Science* **310**, 1626-1627.
- Zografou, S., Basagiannis, D., Papafotika, A., Shirakawa, R., Horiuchi, H., Auerbach, D., Fukuda, M. and Christoforidis, S. (2012). A complete Rab screening reveals novel insights in Weibel-Palade body exocytosis. *J. Cell Sci.* **125**, 4780-4790.